Periodico di Mineralogia
ISSN: 0369-8963

Effects of uniform and non-uniform salinity profiles on the onset of double diffusive Rayleigh-Benard convection in a composite system bounded by rigid-free boundaries with Soret effects and constant heat sources

[1]Somalatha. M. T., [2,]*Archana. M. A., [3]Sumithra. R., [4,a]Vedha. V. R., [4,b]Varshitha. Y. N., [4,c]Anil Kumar. T. V., [4,d]Chandan. M
[1,2,3,4] Department of UG, PG Studies and Research in Mathematics,
Government Science College Autonomous, Bengaluru, Karnataka, India
Corresponding author: [2,*]Archana. M. A.

Abstract

The onset of double diffusive Rayleigh-Benard convection (DD-RBC) in a composite system comprising an incompressible fluid saturated densely packed porous layer over which lies a layer of the same fluid with Soret effect and constant heat sources is investigated. The lower rigid surface of the porous layer and the upper free surface of the fluid layer are insulating to heat and mass. The resulting eigen value problem is solved using regular perturbation technique with wave number as a perturbation parameter. The expression for the Critical Rayleigh number(CRN) is obtained for Linear (LSP), Parabolic (PSP) and Inverted parabolic (IPSP) salinity profiles. The effect of variation of different dimensionless parameters on the onset of DD-RBC is discussed.

Keywords: Double diffusive convection, Composite system, Soret effect, Heat source.

1 Introduction

Double diffusive Rayleigh-Benard convection in a composite fluid-porous system involves buoyancy-driven flow due to gradients in both temperature and solute concentration. This phenomenon has several practical applications across various scientific and engineering disciplines, such as, mantle convection, groundwater contamination and transport, saline intrusion in coastal Aquifers, carbon sequestration, salt fingering and layering, crystal growth and material processing. The onset of finger convection in a porous layer beneath a fluid layer has been examined by Chen and Chen (1988) using linear stability analysis. Chen (1992) investigates salt-finger instability in a fluid layer, bounded above by a rigid wall and below by anisotropic and inhomogeneous porous media, using linear stability analysis. Chen and Su (1992) investigated double diffusive convection with surface tension effects and showed that at low gravity levels, the stability boundary changes drastically due to buoyancy effects, and salt-finger instability may onset in an overstable mode due to the stabilizing effect of surface tension. Gobin et al. (1998) investigated buoyancy driven thermosolutal in a fluid-porous system, using a one-domain formulation. The numerical results on thermosolutal natural convection in a binary fluid contained in a rectangular enclosure, partitioned into porous and fluid vertical layers. Singh et al. (1999) examined heat and mass transfer in a composite fluid - porous cavity, using the Brinkman-Forchheimer-extended Darcy model where vertical walls are isothermal, and horizontal walls are adiabatic. Mahrazi et al. (2000) investigated numerically the natural thermosolutal convection in a cavity with central porous layer flanked by two binary fluid regions, with permeable interface considering extended Darcy-Brinkman law. Zhao and Chen (2001) discussed the results of thermal and salt-finger convection using

https://doi.org/10.5281/zenodo.15486315

one-model equation determining the onset of thermosolutal convection in fluid-porous system. Using one-domain approach and linear stability analysis, Hirata et al. (2009) investigated the onset of double diffusive buoyancy driven convection in a superposed fluid and sparsely packed porous layer, and found that at large wave number, convective instability is confined to fluid layer and at small wave number the instability is confined to porous cavity. Thermal gradients and horizontal solutal effects in a fluid-porous composite medium with impermeable, adiabatic walls are analyzed using the Darcy-Brinkman-Forchheimer model and single domain approach has been studied by Jena et al. (2013). Gangadharaiah (2021) investigated double-diffusive Marangoni convection in a system consisting of a horizontal binary fluid layer over an anisotropic porous matrix.

The presence of heat sources or sinks can significantly impact the flow characteristics, stability and energy transport within the system. Its presence in DD-RBC significantly impacts the flow characteristics of the system. This effect is relevant in geophysical, astrophysical, and engineering applications, such as magma dynamics, nuclear reactor cooling, and oceanic convection. Haajizadeh et al. (1984) and Rao and Wang (1991) investigated a homogeneous heat-generation term inside an enclosure characterised by isothermal vertical walls and adiabatic horizontal walls. The initiation of convection in a fluid permeating a horizontal layer of an anisotropic porous media with an internal heat source, influenced by an inclined temperature gradient, was examined by Parthiban and Palil (1997). Chamka (2002) numerical investigated the double-diffusive convective laminar flow of a binary gas-particle mixture within a rectangular porous enclosure, considering cooperating temperature and concentration gradients along with heat generation or absorption effects. Numerical and analytical investigation of double-diffusive convection with solute-based heat source in a densely packed fluid-saturated porous medium was conducted by Hill (2005). Joshi et al. (2006) provided an analytical solution for low Rayleigh numbers in a finite container with isothermal walls and homogeneous heat production in the porous medium. Magyari et al. (2007a, b) investigated boundary-layer flows in porous media characterized by substantial Rayleigh numbers and internal heat production. Teamah (2008) utilized a horizontal magnetic field to study heat and mass transfer by natural convective flow of a heat-generating fluid inside a rectangle container under steady-state condition. Bhadauria (2011) investigated linear and nonlinear stability analysis of double diffusive convection in an anisotropic porous layer with an internal heat source, heated and salted below using Darcy model. Capone et al. (2011) examined double-diffusive penetrative convection modelled by internal heating in an anisotropic porous medium with throughflow. Effect of non-uniform temperature gradients on thermosolutal convection with Marangoni effects and constant heat source in a composite system was studied by Manjunatha et al. (2021). Sumithra et al. (2022) investigated double diffusive Marangoni convection in a fluid-porous system with variable heat sources. The Soret effect is most often observed in binary mixtures, where different components move in response to a temperature gradient leading to concentration variations across the fluid. The Soret effect is essential in a wide variety of fields, such as, oceanography, chemical and petroleum engineering, microfluidic devices, food processing and geophysics. The linear stability theory on the onset of two-component convection in a fluid layer with Soret effect has been studied by Schechter et al. (1972) and Takashima (1976). Hardin et al. (1990) and Hardin and Sani (1993) investigated linear and weakly non-linear thermosolutal instabilities of binary fluid in a vertical circular cylinder with Soret effects using Galerkin technique. The solutocapillary and thermocapillary instabilities under microgravity in a binary fluid with Soret effect has been analyzed by Joo (1995). Parvathy and Patil (1997) investigated the impact of thermal diffusion on an unbounded, vertically stratified, thermohaline convection in a fluid layer with horizontal salinity and temperature gradients, exploring both stationary and oscillatory modes. The impact of cross diffusion on the double diffusive convection in a two-component system that is

 https://doi.org/10.5281/zenodo.15486315

unbounded and vertically stratified, with compensating horizontal heat and solute gradients was investigated by Malashetty and Gaikwad (2002). The Soret effect in a shallow horizontal porous layer with vertical temperature gradient is studied theoretically using Brinkman‐Hazen‐Darcy model by Bourich et al. (2004). Kim et al. (2007) investigated the convective instabilities of Dufour and Soret effects in a binary nanofluid using linear stability theory. Free convection in a binary mixture with a variable Soret coefficient is analysed linearly by Mojtabi et al (2007). The effects of thermal diffusion on double diffusive Marangoni convection and Rayleigh-Benard convection in a composite system for Darcy and Darcy-Brinkman models, respectively, were investigated by Sumithra et al. (2020, 2022).

The objective of the present problem is to investigate the effects of uniform and nonuniform salinity gradients on the onset of double-diffusive Rayleigh-Benard convection in a composite system. This system is bounded by rigid-free boundaries, incorporates the Soret effect (temperature-induced solute diffusion), and uses the Darcy model for fluid flow through porous media, with constant heat sources in both the layers.

2 Formulation of the Problem

Consider an infinite horizontal incompressible fluid saturated porous layer of thickness $d_m$underlying a layer of the same fluid of thickness d with Soret effect and constant heat sources. The upper free and lower rigid boundaries are subjected to adiabatic temperature and concentration boundary conditions. A Cartesian coordinate system is chosen such that the origin is at the interface and z-axis vertically upwards. The temperatures of the lower and upper boundaries are taken as T_L and T_U respectively, with $T_U < T_L$. The solutes of the lower and upper boundaries are taken as C_L and C_U respectively, with $C_U < C_L$.
The equations governing the fluid layer are:

$$\boldsymbol{\nabla \cdot \overrightarrow{q_f} = 0} \tag{2.1}$$

$$\boldsymbol{\rho_0\left(\frac{\partial \overrightarrow{q_f}}{\partial t} + (\overrightarrow{q_f}\cdot\nabla)\overrightarrow{q_f}\right) = -\nabla P_f + \mu\nabla^2\overrightarrow{q_f} - \rho g\hat{k}} \tag{2.2}$$

$$\boldsymbol{\frac{\partial T_f}{\partial t} + (\overrightarrow{q_f}\cdot\nabla)T_f = \kappa_f\nabla^2 T_f + Q_f} \tag{2.3}$$

$$\boldsymbol{\frac{\partial C_f}{\partial t} + (\overrightarrow{q_f}\cdot\nabla)C_f = \kappa_c\nabla^2 C_f + \kappa_T\nabla^2 T_f} \tag{2.4}$$

$$\boldsymbol{\rho = \rho_0[1 - \alpha_T(T_f - T_0) + \alpha_s(C_f - C_0)]} \tag{2.5}$$

The equations governing the porous layer are:

$$\boldsymbol{\nabla_m \cdot \overrightarrow{q_m} = 0} \tag{2.6}$$

$$\boldsymbol{\frac{\rho_0}{\emptyset}\left(\frac{\partial \overrightarrow{q_m}}{\partial t} + (\overrightarrow{q_m}\cdot\nabla_m)\overrightarrow{q_m}\right) = -\nabla_m P_m - \frac{\mu}{K}\overrightarrow{q_m} - \rho_m g\hat{k}} \tag{2.7}$$

 https://doi.org/10.5281/zenodo.15486315

$$A\frac{\partial T_m}{\partial t} + (\overrightarrow{q_m} \cdot \nabla_m)T_m = \kappa_m \nabla_m^2 T_m + Q_m \tag{2.8}$$

$$\emptyset\frac{\partial C_m}{\partial t} + (\overrightarrow{q_m} \cdot \nabla_m)C_m = \kappa_{cm} \nabla_m^2 C_m + \kappa_{mT} \nabla_m^2 T_m \tag{2.9}$$

$$\rho_m = \rho_0[1 - \alpha_{Tm}(T_m - T_0) + \alpha_{sm}(C_m - C_0)] \tag{2.10}$$

Where $\overrightarrow{q_f} = (u_f, v_f, w_f)$ and $\overrightarrow{q_m} = (u_m, v_m, w_m)$ are the velocity vectors, μ is the fluid viscosity, P is the total pressure, t is the time, $\emptyset$ is the porosity, κ_f and κ_m are respectively the thermal diffusivities of the fluid and porous medium, $A = \frac{(\rho_0 C_p)_m}{(\rho_0 C_p)_f}$ is the ratio of heat capacities, C_p is the specific heat, T_f and T_m respectively denote the temperatures in the fluid and porous layers. $Q_f$and Q_m denotes heat sources, K denotes permeability of the porous medium, ρ_0 is the fluid density at the reference temperature T_0, g is the acceleration due to gravity acting vertically downwards. $C_f$and C_m are species concentrations in fluid and porous layers respectively, κ_c and κ_{cm} are the solute diffusivities in fluid and porous layers respectively. κ_T and κ_{mT} represents Soret coefficients in fluid and porous layers respectively. The subscripts $'m'$, 'f' and 's' refer to the porous, fluid and solid mediums respectively.

The basic steady state is assumed to be quiescent, and pressure, concentration, temperature are functions of z only. We consider the solution in the form.

$$\overrightarrow{q_f} = \overrightarrow{q_{fb}} = 0, P_f = P_{fb}(z_f), C_f = C_{fb}(z_f), T_f = T_{fb}(z_f) \tag{2.11}$$

$$\overrightarrow{q_m} = \overrightarrow{q_{mb}} = 0, P_m = P_{mb}(z_m), C_m = C_{mb}(z_m), T_m = T_{mb}(z_m) \tag{2.12}$$

The temperature distributions $T_{fb}(z_f)$ and $T_{mb}(z_m)$are found to be

$$T_{fb}(z_f) = T_0 + \frac{(T_U - T_0)z_f}{d_f} + \frac{Q_f z_f(d_f - z_f)}{2\kappa_f} \tag{2.13}$$

$$T_{mb}(z_f) = T_0 + \frac{(T_0 - T_L)z_m}{d_m} + \frac{Q_m z_m(d_m - z_m)}{2\kappa_m} \tag{2.14}$$

Where the interface temperature T_0 is given by

$$T_0 = \frac{2(\kappa_f T_U d_m + \kappa_m T_L d_f) + Q_f d_f^2 d_m + d_f Q_m d_m^2}{2(\kappa_f d_m + \kappa_m d_f)} \tag{2.15}$$

The concentration distributions C_{fb} and C_{mb} are found to be

$$C_{fb}(z_f) = C_0 + \left[\frac{(C_U - C_0)z_f}{d_f} - \frac{\lambda Q_f z_f(d_f - z_f)}{2}\right] f(z_f) \tag{2.16}$$

$$C_{mb}(z_m) = C_0 + \left[\frac{(C_0 - C_L)z_m}{d_m} - \frac{\lambda_m Q_m z_m(d_m - z_m)}{2}\right] f_m(z_m) \tag{2.17}$$

where $f(z_f)$ and $f_m(z_m)$ are dimensionless gradient functions, and C_0, the interface concentration is given by

$$C_0 = \frac{2(d_m \kappa_c C_U + d_f \kappa_m C_L) - \lambda \kappa_c Q_f d_m d_f^2 - d_f \kappa_{mc} \lambda_m Q_m d_m^2}{(\kappa_f d_m + \kappa_m d_f)} \tag{2.18}$$

To investigate the stability analysis of the basic solution, perturbations are superimposed in the form:

$$\overrightarrow{q_f} = \overrightarrow{q_{fb}} + \overrightarrow{q_f}', P_f = P_{fb}(z_f) + P_f', C_f = C_{fb}(z_f) + s_f, T_f = T_{fb}(z_f) + \theta_f \tag{2.19}$$

 https://doi.org/10.5281/zenodo.15486315

$$\left.\begin{array}{c}\overrightarrow{\boldsymbol{q_m}} = \overrightarrow{\boldsymbol{q_{mb}}} + \overrightarrow{\boldsymbol{q_m}}', \boldsymbol{P_m} = \boldsymbol{P_{mb}}(\boldsymbol{z_m}) + \boldsymbol{P'_m}, \boldsymbol{C_m} = \boldsymbol{C_{mb}}(\boldsymbol{z_m}) + \boldsymbol{s_m}, \\ \boldsymbol{T_m} = \boldsymbol{T_{mb}}(\boldsymbol{z_m}) + \boldsymbol{\theta_m}\end{array}\right\} \quad (2.20)$$

The above equations are substituted in equations (2.1) to (2.10) and linearized in the usual manner. By taking curl twice on equations (2.2) and (2.7), the pressure terms are eliminated, only the vertical components are retained. Separate length scales are used for the fluid and porous layers in order to render the equations non-dimensional, ensuring that both layers have a unit depth and are:

$$\left.\begin{array}{c}\left(\boldsymbol{u_f}, \boldsymbol{v_f}, \boldsymbol{w_f}\right) = \dfrac{\boldsymbol{\kappa_f}}{\boldsymbol{d_f}}\left(\boldsymbol{u_f^*}, \boldsymbol{v_f^*}, \boldsymbol{w_f^*}\right), \boldsymbol{\theta_f} = (\boldsymbol{T_0} - \boldsymbol{T_U})\boldsymbol{\theta_f^*}, \boldsymbol{t_f} = \dfrac{\boldsymbol{d_f^2}}{\boldsymbol{\kappa_f}}\boldsymbol{t_f^*}, \boldsymbol{\nabla_f} = \dfrac{\boldsymbol{\nabla_f^*}}{\boldsymbol{d_f}}, \\ \left(\boldsymbol{x_f}, \boldsymbol{y_f}, \boldsymbol{z_f}\right) = \boldsymbol{d_f}\left(\boldsymbol{x_f^*}, \boldsymbol{y_f^*}, \boldsymbol{z_f^*}\right), \boldsymbol{s_f} = (\boldsymbol{C_0} - \boldsymbol{C_U})\boldsymbol{s_f^*}\end{array}\right\} \quad (2.21)$$

$$\left.\begin{array}{c}(\boldsymbol{u_m}, \boldsymbol{v_m}, \boldsymbol{w_m}) = \dfrac{\boldsymbol{\kappa_m}}{\boldsymbol{d_m}}(\boldsymbol{u_m^*}, \boldsymbol{v_m^*}, \boldsymbol{w_m^*}), \boldsymbol{\theta_m} = (\boldsymbol{T_L} - \boldsymbol{T_0})\boldsymbol{\theta_m^*}, \boldsymbol{t_m} = \dfrac{\boldsymbol{d_m^2}}{\boldsymbol{\kappa_m}}\boldsymbol{t_m^*}, \\ \boldsymbol{\nabla_m} = \dfrac{\boldsymbol{\nabla_m^*}}{\boldsymbol{d_m}}, (\boldsymbol{x_m}, \boldsymbol{y_m}, \boldsymbol{z_m}) = \boldsymbol{d_m}(\boldsymbol{x_m^*}, \boldsymbol{y_m^*}, \boldsymbol{z_m^*} - \boldsymbol{1}), \boldsymbol{s_m} = (\boldsymbol{C_L} - \boldsymbol{C_0})\boldsymbol{s_m^*}\end{array}\right\} \quad (2.22)$$

The linearized non-dimensional equations are:

$$\frac{\boldsymbol{1}}{\boldsymbol{Pr_f}}\frac{\boldsymbol{\partial}\left(\boldsymbol{\nabla_f^2 w_f}\right)^{\boldsymbol{2}}}{\boldsymbol{\partial t_f}} = \boldsymbol{\nabla_f^4 w_f} + \boldsymbol{Ra_T}\boldsymbol{\nabla_{2f}^2}\boldsymbol{\theta_f} - \boldsymbol{Ra_S}\boldsymbol{\nabla_{2f}^2}\boldsymbol{s} \quad (2.23)$$

$$\frac{\boldsymbol{\partial \theta_f}}{\boldsymbol{\partial t_f}} - \boldsymbol{w_f} - \boldsymbol{Q_f}\frac{\left(\boldsymbol{2z_f} - \boldsymbol{1}\right)\boldsymbol{d_f^2 w_f}}{\boldsymbol{2\kappa_f}(\boldsymbol{T_0} - \boldsymbol{T_U})} = \boldsymbol{\nabla_f^2 \theta_f} \quad (2.24)$$

$$\left.\begin{array}{c}\dfrac{\boldsymbol{\partial s_f}}{\boldsymbol{\partial t_f}} - \boldsymbol{w_f} + \dfrac{\boldsymbol{\lambda Q_f d_f^2}\left(\boldsymbol{2z_f} - \boldsymbol{1}\right)\boldsymbol{w_f}}{\boldsymbol{2}(\boldsymbol{C_0} - \boldsymbol{C_U})} = \boldsymbol{\tau_f}\boldsymbol{\nabla_f^2 s} + \boldsymbol{\tau_T}\dfrac{(\boldsymbol{T_0} - \boldsymbol{T_U})}{(\boldsymbol{C_0} - \boldsymbol{C_U})}\boldsymbol{\nabla_f^2}\boldsymbol{\theta_f}\end{array}\right\} \quad (2.25)$$

$$\frac{\boldsymbol{\beta^2}}{\boldsymbol{Pr_m}}\frac{\boldsymbol{\partial w_m}}{\boldsymbol{\partial t_m}} = -\boldsymbol{\nabla_m^2 w_m} + \boldsymbol{Ra_m}\boldsymbol{\nabla_{2m}^2}\boldsymbol{\theta_m} - \boldsymbol{Ra_{sm}}\boldsymbol{\nabla_{2m}^2}\boldsymbol{s_m} \quad (2.26)$$

$$\boldsymbol{A}\frac{\boldsymbol{\partial \theta_m}}{\boldsymbol{\partial t_m}} - \boldsymbol{w_m}\frac{\boldsymbol{Q_m}(\boldsymbol{2z_m} + \boldsymbol{1})}{\boldsymbol{2\kappa_m}(\boldsymbol{T_L} - \boldsymbol{T_0})} = \boldsymbol{\nabla_m^2 \theta_m} \quad (2.27)$$

$$\boldsymbol{\phi}\frac{\boldsymbol{\partial s_m}}{\boldsymbol{\partial t_m}} - \boldsymbol{w_m} + \frac{\boldsymbol{\lambda_m Q_m d_m^2}(\boldsymbol{2z_m} - \boldsymbol{1})\boldsymbol{w_m}}{\boldsymbol{2}(\boldsymbol{C_L} - \boldsymbol{C_0})} = \boldsymbol{\tau_c}\boldsymbol{\nabla_m^2 s_m} + \boldsymbol{\tau_{cT}}\frac{(\boldsymbol{T_0} - \boldsymbol{T_U})}{(\boldsymbol{C_0} - \boldsymbol{C_U})}\boldsymbol{\nabla_m^2}\boldsymbol{\theta_m} \quad (2.28)$$

where $Pr_f = \frac{\mu}{\rho_0 \kappa_f}$, $\beta^2 = Da = \frac{K}{d_m^2}$, $Ra_T = \frac{\alpha_f g(T_0 - T_U)}{\nu \kappa_f}$, $Pr_m = \frac{\phi \nu}{\kappa_m}$, $Ra_m = \frac{\alpha_m g(T_L - T_0) d_m K}{\nu_m \kappa_m}$, $Ra_s = \frac{g\alpha_s(C_0 - C_U)d_f^3}{\nu \kappa_c}$, $Ra_{sm} = \frac{\alpha_{sm} g(C_L - C_0) d_m^3}{\nu_m \kappa_{cm}}$ are Prandtl number in fluid layer, Darcy number, thermal Rayleigh number in fluid layer, Prandtl number in porous layer, thermal Rayleigh number in porous layer, solute Rayleigh number in fluid layer, and solute Rayleigh number in porous layer. Here $\nu = \frac{\mu}{\rho_0}$ and ν_m is effective viscosity in porous layer.

Normal Mode Expansion

Carrying out the following normal mode analysis on the dimensionless equations, the

$$\begin{bmatrix}\boldsymbol{w_f} \\ \boldsymbol{\theta_f} \\ \boldsymbol{s_f}\end{bmatrix} = \begin{bmatrix}\boldsymbol{W_f}(\boldsymbol{z_f}) \\ \boldsymbol{\Theta_f}(\boldsymbol{z_f}) \\ \boldsymbol{S_f}(\boldsymbol{z_f})\end{bmatrix}\boldsymbol{g}(\boldsymbol{x_f}, \boldsymbol{y_f})\boldsymbol{e^{\eta_f t_f}} \quad (2.29)$$

 https://doi.org/10.5281/zenodo.15486315

ISSN: 0369-8963

$$\begin{bmatrix} w_m \\ \theta_m \\ s_m \end{bmatrix} = \begin{bmatrix} W_f(z_m) \\ \Theta_f(z_m) \\ S_f(z_m) \end{bmatrix} g_m(x_m, y_m) e^{\eta_m t_m} \tag{2.30}$$

Subsequent ordinary differential equations obtained are:

$$\left(D_f^2 - a_f^2\right)^2 W_f(z_f) + \frac{\eta_f}{Pr_f}\left(D_f^2 - a_f^2\right) W_f(z_f) = a_f^2\left[Ra_T \Theta_f(z_f) - Ra_S S_f(z_f)\right] \tag{2.31}$$

$$\left(\left(D_f^2 - a_f^2\right) + \eta_f\right)\Theta_f(z_f) + W_f(z_f) + \frac{Q_f d_f^2 (2z_f - 1)}{2\kappa_f (T_0 - T_U)} W_f(z_f) = 0 \tag{2.32}$$

$$\left.\begin{aligned} \left(\tau_f\left(D_f^2 - a_f^2\right) + \eta_f\right) S_f(z_f) f(z_f) + \frac{Q_f \lambda d_f^2 (2z_f - 1)}{2\kappa_f (C_0 - C_U)} W_f(z_f) \\ + W_f(z_f) + Sr_f\left(D_f^2 - a_f^2\right)\Theta_f(z_f) \end{aligned}\right\} = 0 \tag{2.33}$$

$$\left[\frac{\beta^2}{Pr_m} - 1\right]\left(D_m^2 - a_m^2\right) W_m(z_m) = a_m^2 [Ra_m \Theta_m(z_m) - Ra_{Sm} S_m(z_m)] \tag{2.34}$$

$$\left(\left(D_m^2 - a_m^2\right) + \phi\eta_m\right)\Theta_m(z_m) + W_m(z_m) + \frac{Q_m d_m^2 (2z_m + 1)}{2\kappa_m (T_L - T_0)} W_m(z_m) = 0 \tag{2.35}$$

$$\left.\begin{aligned} \left(\tau_m\left(D_m^2 - a_m^2\right) + \phi\eta_m\right) S_m(z_m) f_m(z_m) - \frac{Q_m \lambda_m d_m^2 (2z_m + 1)}{2\kappa_m (C_0 - C_U)} W_m(z_m) \\ + W_m(z_m) + Sr_m\left(D_m^2 - a_m^2\right)\Theta_m(z_m) \end{aligned}\right\} = 0 \tag{2.36}$$

Since the principle of exchange of stability holds for the given problem, time derivatives are neglected. That is, $\eta_f = \eta_m = 0$. Thus, the convection manifests itself as stationary convection directly, and the equations (2.31) to (2.36) reduces to the following form:

$$\left(D_f^2 - a_f^2\right)^2 W_f(z_f) = a_f^2\left[Ra_T \Theta_f(z_f) - Ra_S S_f(z_f)\right] \tag{2.37}$$

$$\left(D_f^2 - a_f^2\right)\Theta_f(z_f) + W_f(z_f) + R_I^*(2z_f - 1) W_f(z_f) = 0 \tag{2.38}$$

$$\left.\begin{aligned} \left(D_f^2 - a_f^2\right) S_f(z_f) f(z_f) + \frac{1}{\tau_f}\left[1 + \lambda(2z_f - 1)\right] W_f(z_f) \\ + Sr_f\left(D_f^2 - a_f^2\right)\Theta_f(z_f) \end{aligned}\right\} = 0 \tag{2.39}$$

$$\left(D_m^2 - a_m^2\right) W_m(z_m) = a_m^2 [Ra_m \Theta_m(z_m) - Ra_{Sm} S_m(z_m)] \tag{2.40}$$

$$\left(D_m^2 - a_m^2\right)\Theta_m(z_m) + W_m(z_m) + R_{Im}^*(2z_m + 1) W_m(z_m) = 0 \tag{2.41}$$

$$\left.\begin{aligned} \left(D_m^2 - a_m^2\right) S_m(z_m) f_m(z_m) + \frac{1}{\tau_m}\left[1 - \lambda_m(2z_m + 1)\right] W_m(z_m) \\ + Sr_m\left(D_m^2 - a_m^2\right)\Theta_m(z_m) \end{aligned}\right\} = 0 \tag{2.42}$$

where $R_I^* = \frac{Q_f d_f^2}{2\kappa_f (T_0 - T_U)}$ and $R_{Im}^* = \frac{Q_m d_m^2}{2\kappa_m (T_L - T_0)}$ are respectively modified internal Rayleigh numbers in fluid and porous layers, $Sr_f = \frac{\tau_T (T_0 - T_U)}{\tau_f (C_0 - C_U)}$ and $Sr_m = \frac{\tau_{CT} (T_L - T_0)}{\tau_m (C_L - C_0)}$ are respectively Soret parameters in fluid and porous layers. D_f and D_m are differential operators with respect to z_f

 https://doi.org/10.5281/zenodo.15486315

and z_m. If the matching of the solution in the two layers is possible, the wave number must be the same for the fluid and porous layer, so that we have $\frac{a_f}{a_m} = \frac{d_f}{d_m}$

Boundary conditions

To solve the equations (2.37) to (2.42), we impose the following boundary conditions (after implementing non-dimensionalization and normal mode analysis).
Velocity boundary conditions are:

$$\left.\begin{gathered} \boldsymbol{W_f(1) = 0; D_f^2 W_f(1) = 0;\ \epsilon_T \hat{d} W_f(0) = W_m(1);\ W_m(0) = 0} \\ \boldsymbol{\hat{d}^3 \epsilon_T \left(D_f^2 + a_f^2\right) W_f(0) = \left(D_m^2 + a_m^2\right) W_m(1);} \\ \boldsymbol{\hat{d}^4 \epsilon_T Da \left(D_f^3 - 3a_f^2 D_f\right) W_f(0) + D_m W_m(1) = 0} \end{gathered}\right\} \quad (2.43)$$

Temperature boundary conditions are:

$$\boldsymbol{D_f \Theta_f(1) = 0;\ \Theta_f(0) = \hat{d} \epsilon_T \Theta_m(1);\ D_f \Theta_f(0) = D_m \Theta_m(1);\ D_m \Theta_m(0) = 0} \quad (2.44)$$

Salinity boundary conditions are:

$$\boldsymbol{D_f S_f(1) = 0;\ S_f(0) = \hat{d} \epsilon_s S_m(1);\ D_f S_f(0) = D_m S_m(1);\ D_m S_m(0) = 0} \quad (2.45)$$

where $\hat{d} = \frac{d_m}{d_f}$ is the depth ratio, $\epsilon_T = \frac{\kappa_f}{\kappa_m}$ is thermal diffusivity ratio, $\epsilon_s = \frac{\kappa_c}{\kappa_{cm}}$ is solute diffusivity ratio.

3 Solution by regular perturbation technique:

To validate tiny wave number analysis, the dependent variables in both fluid and porous layers are presented in powers of a_f^2, as follows:

$$\left(\boldsymbol{W_f(z_f), \Theta_f(z_f), S_f(z_f)}\right) = \sum_{\boldsymbol{i=0}}^{\infty} \left(\boldsymbol{a_f^2}\right)^{\boldsymbol{i}} \left(\boldsymbol{W_{fi}(z_f), \Theta_{fi}(z_f), S_{fi}(z_f)}\right) \quad (3.1)$$

$$\left(\boldsymbol{W_m(z_m), \Theta_m(z_m), S_m(z_m)}\right) = \sum_{\boldsymbol{i=0}}^{\infty} \left(\boldsymbol{\hat{d}^2 a_f^2}\right)^{\boldsymbol{i}} \left(\boldsymbol{W_{mi}(z_m), \Theta_{mi}(z_m), S_{mi}(z_m)}\right) \quad (3.2)$$

Substituting the above equations into equations (2.37) to (2.42) yields a sequence of equations for the unknown functions $\left(W_{fi}(z_f), \Theta_{fi}(z_f), S_{fi}(z_f)\right)$ and $(W_{mi}(z_m), \Theta_{mi}(z_m), S_{mi}(z_m))$ for $i = 0, 1, 2, 3, \ldots\ldots$
The solutions to zeroth order equations satisfying zeroth order boundary conditions are:

$$\left.\begin{gathered} \boldsymbol{W_{f_0}(z_f) = 0 = W_{m_0}(z_m), \Theta_{f_0}(z_f) = \hat{d} \epsilon_T,} \\ \boldsymbol{\Theta_{m_0}(z_m) = 1, S_{f_0}(z_f) = \hat{d} \epsilon_s, S_{m_0}(z_m) = 1} \end{gathered}\right\} \quad (3.3)$$

The solutions of the velocity equations (2.37) and (2.40) of order a_f^2, satisfying corresponding boundary conditions (2.43) of the same order are:

$$\boldsymbol{W_{f_1}(z_f) = b_5 + b_6 z_f + b_7 z_f^2 + b_8 z_f^3 + \frac{\hat{d} z_f^4}{24} (\epsilon_T Ra_T - \epsilon_s Ra_S)} \quad (3.4)$$

$$\boldsymbol{W_{m_1}(z_m) = b_9 + b_{10} z_m + \frac{z_f^2}{2} (Ra_m + Ra_{Sm})} \quad (3.5)$$

where $b_5 = \frac{\hat{d}}{\epsilon_T} b_{10} + \frac{\hat{d}}{2\epsilon_T} (Ra_m + Ra_{Sm})$, $b_7 = \frac{1}{2\hat{d}\epsilon_T} (Ra_m + Ra_{Sm})$, $b_9 = 0$,
$b_7 + 3b_8 = \frac{\hat{d}}{4} (\epsilon_s Ra_S - \epsilon_T Ra_T)$, $b_{10} = -\left(6\hat{d}^2 \epsilon_T Da\right) b_8 - (Ra_m + Ra_{Sm})$,

 https://doi.org/10.5281/zenodo.15486315

ISSN: 0369-8963

$$b_5 + b_6 + b_7 + b_8 = -\frac{\hat{d}}{24}(\epsilon_T Ra_T - \epsilon_s Ra_S)$$

The boundary conditions (2.45) and differential equations for concentration (2.39) and (2.42) of order a_f^2 establish the following solvability condition:

$$\frac{\mathbf{1}}{\boldsymbol{\tau_f}}\int_0^1 \left[\mathbf{1} + \boldsymbol{\lambda}(\mathbf{2}\boldsymbol{z_f} - \mathbf{1})\boldsymbol{W_{f_1}}(\boldsymbol{z_f})\boldsymbol{f}(\boldsymbol{z_f})\, \boldsymbol{dz_f}\right] + \frac{\hat{\boldsymbol{d}}^{\mathbf{2}}}{\boldsymbol{\tau_m}}\int_0^1 \left[\mathbf{1} + \boldsymbol{\lambda_m}(\mathbf{2}\boldsymbol{z_m} + \mathbf{1})\boldsymbol{W_{m_1}}(\boldsymbol{z_m})\boldsymbol{f_m}(\boldsymbol{z_m})\, \boldsymbol{dz_m}\right] = \hat{\boldsymbol{d}} + \hat{\boldsymbol{d}}\boldsymbol{\epsilon_s} \tag{3.6}$$

Equation (3.6) is solved for the following salinity gradient functions:

Salinity profile	Gradient function	Critical Rayleigh number
Linear	$f(z_f) = 1, f_m(z_m) = 1$	Ra_{T1}
Parabolic	$f(z_f) = 2z_f, f_m(z_m) = 2z_m$	Ra_{T2}
Inverted Parabolic	$f(z_f) = 2(z_f - 1),$ $f_m(z_m) = 2(z_m - 1)$	Ra_{T3}

3.1 Linear Salinity Profile (LSP):

$$Ra_{T1} = \frac{\hat{d}(\epsilon_s + Sr_f\epsilon_T) + \hat{d}^2(1 + Sr_m) - \mathrm{A}_{s1} - \mathrm{A}_{sm1}}{\mathrm{A}_{T1} + \mathrm{A}_{m1}}$$

$\mathrm{A}_{T1} = \frac{1}{\tau_f}\left\{C_{T4} - C_{T5}\left(\frac{3+\lambda}{6}\right) + C_{T3}\left(\frac{2+\lambda}{6}\right) - C_{T1}\left(\frac{5+3\lambda}{20}\right) + \frac{(3+2\lambda)\hat{d}\epsilon_T}{360}\right\}$, $C_{T1} = \frac{\epsilon_T\hat{d}}{12} + \frac{Da\hat{d}^3\epsilon_T}{6}$

$\mathrm{A}_{sm1} = \frac{\hat{d}^2}{\tau_m}\left(C_{s2} - \frac{(3-7\lambda_m)}{6} + \frac{(2-5\lambda_m)Ra_{sm}}{12}\right)$, $\mathrm{A}_{m1} = \frac{\hat{d}^2}{\tau_m}\left(C_{T2} - \frac{(3-7\lambda_m)}{6} + \frac{(2-5\lambda_m)\epsilon_T^2\hat{d}^4Da}{12}\right)$,

$\mathrm{A}_{s1} = \frac{1}{\tau_f}\left\{C_{s4} - C_{s5}\left(\frac{3+\lambda}{6}\right) + C_{s3}\left(\frac{2+\lambda}{6}\right) + C_{s1}\left(\frac{5+3\lambda}{20}\right) - \frac{(3+2\lambda)Ra_S\epsilon_s\hat{d}}{360}\right\}$, $C_{s1} = \frac{Ra_S\epsilon_s\hat{d}}{12} - \frac{Ra_{sm}}{6\hat{d}\epsilon_T}$,

$C_{s3} = \frac{Ra_{sm}}{2\hat{d}\epsilon_T}$, $C_{T3} = \frac{Da\hat{d}^3\epsilon_T}{2}$, $C_{T2} = Da\hat{d}^2\epsilon_T(6C_{T1} - \hat{d}^2\epsilon_T)$, $C_{s2} = -\left(6Da\hat{d}^2\epsilon_T C_{s1} + Ra_{sm}\right)$

$C_{s4} = \frac{\hat{d}}{2\epsilon_T}(2C_{s2} + Ra_{sm})$, $C_{T4} = \frac{\hat{d}C_{s2}}{\epsilon_T} + \frac{\hat{d}\epsilon_T Da}{2}$, $C_{s5} = C_{s1} + C_{s3} + C_{s4} - \frac{\epsilon_s\hat{d}Ra_S}{24}$,

$C_{T5} = C_{T4} + C_{T3} - C_{T1} + \frac{\epsilon_T\hat{d}}{24}$

3.2 Parabolic Salinity Profile (PSP):

$$Ra_{T2} = \frac{\hat{d}(\epsilon_s + Sr_f\epsilon_T) + \hat{d}^2(1 + Sr_m) - \mathrm{A}_{s2} - \mathrm{A}_{sm2}}{\mathrm{A}_{T2} + \mathrm{A}_{m2}}$$

$\mathrm{A}_{T2} = \frac{2}{\tau_f}\left\{C_{T4}\left(\frac{3+\lambda}{6}\right) + \frac{2+\lambda}{6}C_{T5} + C_{T3}\left(\frac{5+3\lambda}{20}\right) + C_{T1}\left(\frac{3+2\lambda}{15}\right) + \frac{(7+5\lambda)\hat{d}\epsilon_T}{1008}\right\}$,

$\mathrm{A}_{m2} = \frac{2\hat{d}^2}{\tau_m}\left(C_{T2}\frac{(2-5\lambda_m)}{6} + \frac{(5-13\lambda_m)\epsilon_T^2\hat{d}^4Da}{40}\right)$, $\mathrm{A}_{sm2} = \frac{2\hat{d}^2}{\tau_m}\left(C_{s2}\frac{(2-5\lambda_m)}{6} + \frac{(5-13\lambda_m)Ra_{sm}}{40}\right)$,

$$\mathrm{A}_{s2} = \frac{2}{\tau_f}\left\{C_{s4}\left(\frac{3+\lambda}{6}\right) - C_{s5}\left(\frac{2+\lambda}{6}\right) + C_{s3}\left(\frac{5+3\lambda}{20}\right) + C_{s1}\left(\frac{3+2\lambda}{15}\right) - \frac{(7+5\lambda)\hat{d}\epsilon_s Ra_S}{1008}\right\}$$

3.3 Inverted Parabolic Salinity Profile (IPSP):

$$Ra_{T3} = \frac{\hat{d}(\epsilon_s + Sr_f\epsilon_T) + \hat{d}^2(1 + Sr_m) - \mathrm{A}_{s3} - \mathrm{A}_{sm3}}{\mathrm{A}_{T3} + \mathrm{A}_{m3}}$$

$\mathrm{A}_{T3} = \frac{2}{\tau_f}\left\{C_{T4}\left(\frac{3-\lambda}{6}\right) + \frac{C_{T5}}{6} + C_{T3}\left(\frac{5+\lambda}{60}\right) - C_{T1}\left(\frac{3+\lambda}{60}\right) + \frac{(7+3\lambda)\hat{d}\epsilon_T}{5040}\right\}$,

 https://doi.org/10.5281/zenodo.15486315

$$A_{m3} = \frac{2\hat{d}^2}{\tau_m}\left(C_{T2}\frac{(1-2\lambda_m)}{6} + \frac{(5-11\lambda_m)\epsilon_T^2\hat{d}^4 Da}{120}\right), A_{sm3} = \frac{2\hat{d}^2}{\tau_m}\left(C_{s3}\frac{(1-2\lambda_m)}{6} + \frac{(5-11\lambda_m)Ra_{sm}}{120}\right),$$
$$A_{s3} = \frac{2}{\tau_f}\left\{C_{s4}\left(\frac{3-\lambda}{6}\right) - \left(\frac{C_{s5}}{6}\right) + C_{s3}\left(\frac{5+\lambda}{60}\right) + C_{s1}\left(\frac{3+\lambda}{60}\right) - \frac{(7+3\lambda)\hat{d}\epsilon_s Ra_S}{5040}\right\}$$

4 Results and discussion

The effects of uniform and nonuniform salinity gradients on the onset of double diffusive Rayleigh-Benard convection in a composite system with Soret effect and constant heat sources is investigated for upper free and lower rigid velocity boundary conditions. The Critical Rayleigh numbers (CRN) Ra_{T1}, Ra_{T2} and Ra_{T3} are obtained respectively for Linear (LSP), Parabolic (PSP) and Inverted Parabolic (IPSP) salinity profiles.

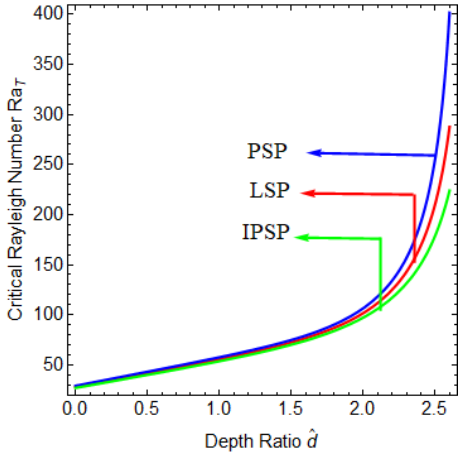

Figure 4.1: Comparison of CRN versus $\hat{d}$ for LSP, PSP and IPSP

Figure 4.1 represents comparison of Linear (LSP), Parabolic (PSP) and Inverted Parabolic (IPSP) salinity profiles for CRN versus $\hat{d}$ when the fixed parameters are $R_I^* = R_{Im}^* = 0.5$, $Da = 0.0001, \epsilon_T = \epsilon_s = Ra_S = 1, Sr_f = Sr_m = -0.1, \tau_f = \tau_m = 0.25$. From the figure, the CRNs, Ra_{T1}, Ra_{T2} and Ra_{T3} respectively for LSP, PSP and IPSP increases gradually with $\hat{d}$. It is observed that Parabolic salinity profile (PSP) is most stable one and Inverted Parabolic (IPSP) is the most unstable salinity profile. Also, the graph reveals that for larger $\hat{d}$ values the curves are diverging, indicating that the profiles are significant in porous layer dominant composite (PLDC) system.

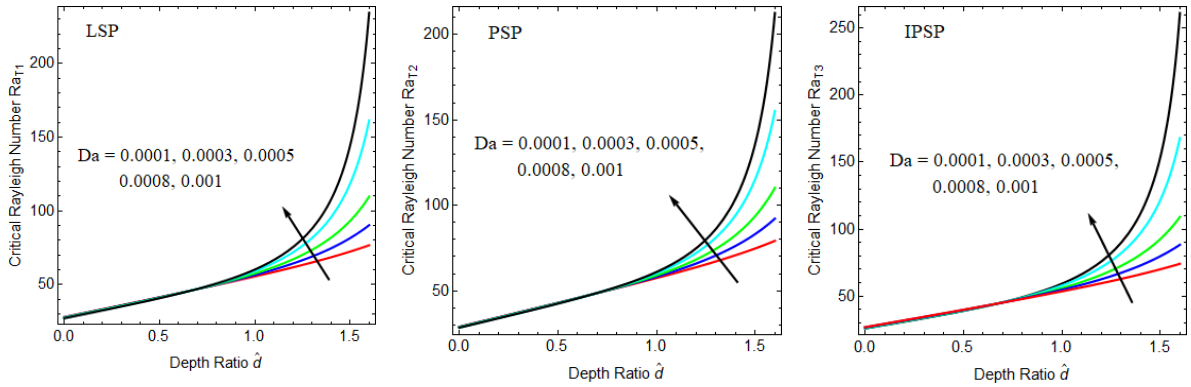

https://doi.org/10.5281/zenodo.15486315

(a) Linear (b) Parabolic (c) Inverted Parabolic

Figure 4.2: Effects of Darcy number Da

Figures 4.2a, 4.2b and 4.2c respectively shows CRN versus $\hat{d}$ for different values of $Da = 0.0001, 0.0003, 0.0005, 0.0008, 0.001$ for LSP, PSP and IPSP. The curves are merging for smaller values of $\hat{d}$ and diverge for larger $\hat{d}$ values. This indicates that the impact of this parameter is substantial in PLDC system which is obvious. Also, the CRNs Ra_{T1}, Ra_{T2} and Ra_{T3} increase with increase in Da. That is, Da shows stabilizing effect of the composite system and hence the onset of DD-RBC is delayed.

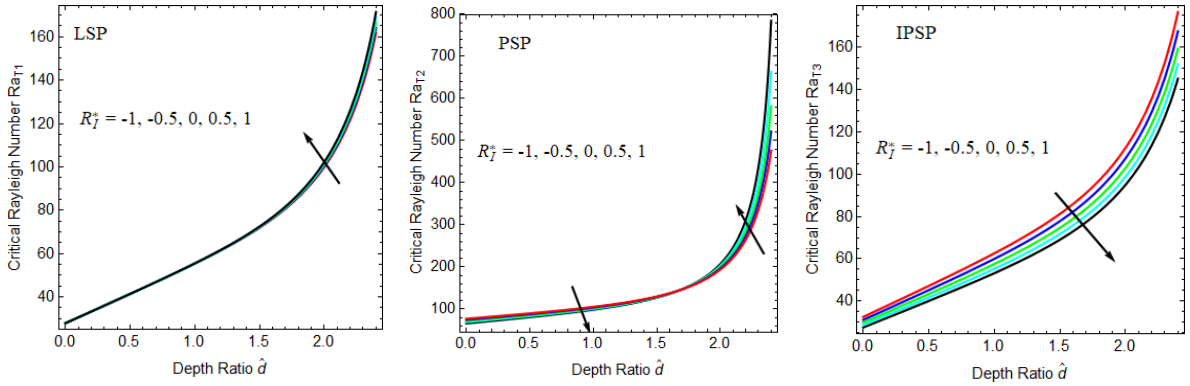

(a) Linear (b) Parabolic (c) Inverted Parabolic

Figure 4.3: Effects of modified internal Rayleigh number in fluid layer R_I^*

Figures 4.3a, 4.3b and 4.3c illustrates the CRN versus $\hat{d}$ for LSP, PSP and IPSP by varying, $R_I^* = -1, -0.5, 0, 0.5, 1$. In case of LSP and PSP, increasing from sink to source, R_I^* increases CRN, showing stabilizing effect and delaying the onset of DD-RB convection. In case of IPSP, increase in R_I^*decreases CRN showing destabilizing effect and hastening the onset of DD-RB convection. In figures 4.3(a)and 4.3(b), the curves are merged initially and diverge slightly for larger values of depth ratio indicating that this parameter is crucial in PLDC system.

Figures 4.4a, 4.4b and 4.4c illustrates the Critical Rayleigh number (CRN) versus depth ratio $\hat{d}$ for Linear, Parabolic and Inverted Parabolic salinity profiles by varying modified internal Rayleigh number in the porous layer, $R_{Im}^* = -1, -0.5, 0, 0.5, 1$(increasing from sink to source). In figures 4.4(a), 4.4(b)and 4.4(c), the curves are merged initially and diverge for larger values of depth ratio, indicating that this parameter is crucial in porous dominant composite system for all the three profiles. Also, increase in R_{Im}^* increases CRNs for all the three profiles showing stabilizing effect and delaying the onset DD-RB convection.

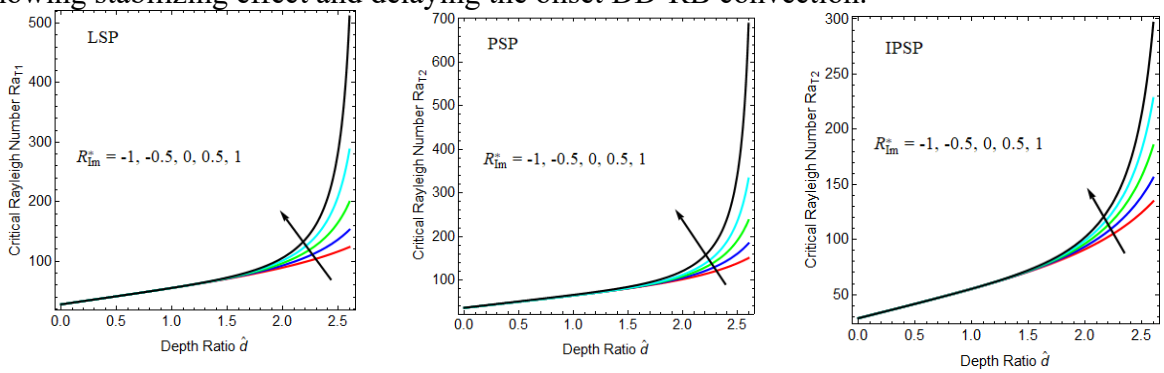

(a)Linear (b)Parabolic (c) Inverted Parabolic

Figure 4.4: Effects of modified internal Rayleigh number in porous layer R_{Im}^*

https://doi.org/10.5281/zenodo.15486315

Figures 4.5a, 4.5b and 4.5c illustrates the Critical Rayleigh number (CRN) versus depth ratio for Linear, Parabolic and Inverted Parabolic salinity profiles by varying Solute Rayleigh number in the fluid layer, $Ra_S = 1, 1.4, 1.8, 2.2, 2.5$. In figures 4.5(a), 4.5(b)and 4.5(c), the curves are merged initially and diverge for larger values of depth ratio indicating that this parameter is crucial in porous dominant composite system for all the profiles considered. Also, increase in Ra_S increases CRNs for all the three profiles showing stabilizing effect and delaying the onset DD-RBC convection.

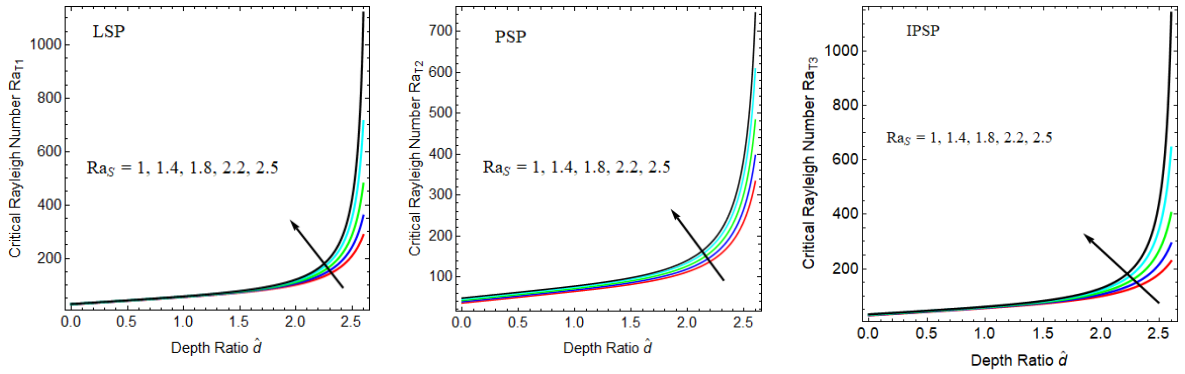

(a)Linear (b)Parabolic (c) Inverted Parabolic

Figure 4.5: Effects of Solute Rayleigh number in fluid layer Ra_S

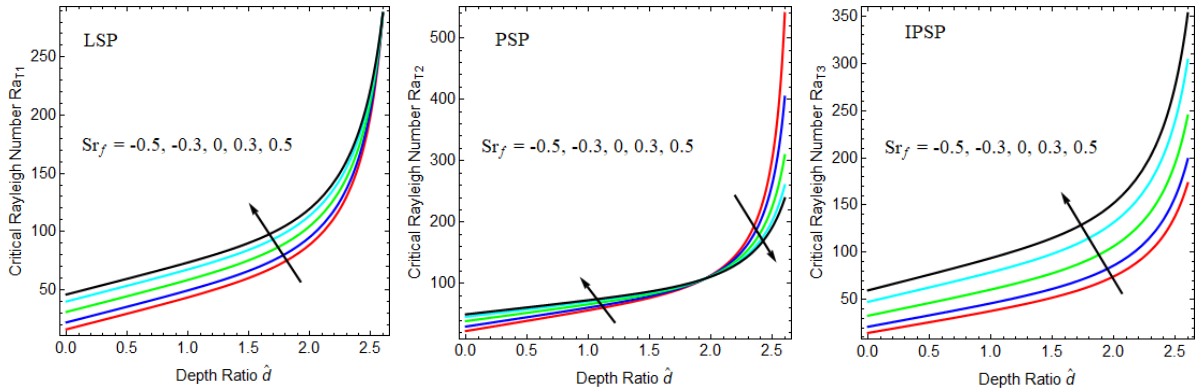

(a)Linear (b)Parabolic (c) Inverted Parabolic

Figure 4.6: Effects of Soret parameter in fluid layer Sr_f

Figures 4.6(a), 4.6(b)b and 4.6(c) illustrates the Critical Rayleigh number (CRN) versus depth ratio for Linear, Parabolic and Inverted Parabolic salinity profiles by varying Soret parameter in the fluid layer, $Sr_f = -0.5, -0.3, 0, 0.3, 0.5$. Increase in$Sr_f$ increases CRNs, Ra_{T1} and Ra_{T3} for Linear and inverted parabolic salinity profiles as shown in figures 4.6(a) and 4.6(c). That is, Sr_f stabilizes the composite system and delays the onset of DDRB convection for Linear and Inverted Parabolic salinity profiles. In case of Parabolic salinity profile, a dual effect is observed, i.e., for $0 \leq \hat{d} \leq 2$, increase in Sr_f increases CRN, Ra_{T2} showing stabilizing effect and for $2 \leq \hat{d} \leq 2.6$, increase in Sr_f decreases CRN, Ra_{T2} showing destabilizing effect. This indicates that depth ratio plays a crucial role and this parameter is sensitive to changes in depth ratio. Therefore, by selecting suitable salinity profile and range of depth ratio, the composite system onset of convection can be delayed or hastened. Also, in fig 4.6(a), the curves are converging for larger values of depth ratio, indicating that this parameter is crucial for fluid dominant composite system in case of LSP.

https://doi.org/10.5281/zenodo.15486315

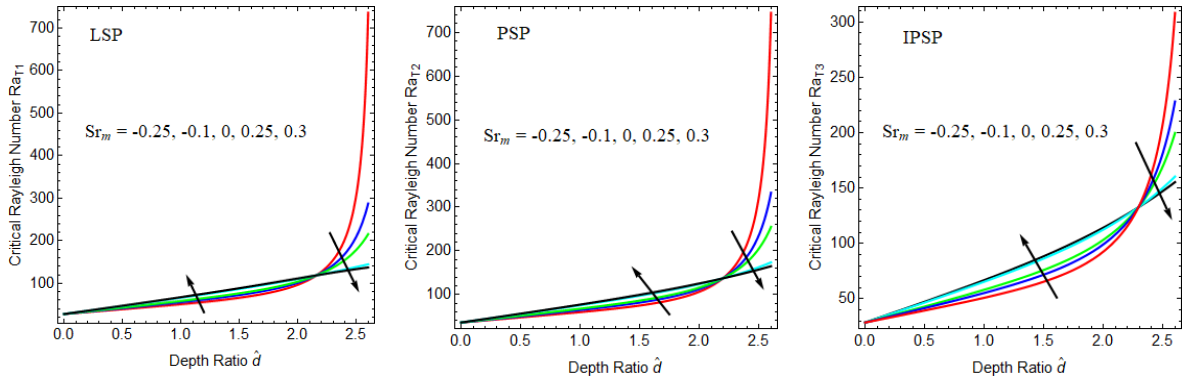

(a)Linear (b)Parabolic (c) Inverted Parabolic

Figure 4.7: Effects of Soret parameter in porous layer Sr_m

Figures 4.7a, 4.7b and 4.7c illustrates the Critical Rayleigh numbers (CRNs) Ra_{T1}, Ra_{T2} and Ra_{T3} versus depth ratio for Linear, Parabolic and Inverted Parabolic salinity profiles by varying Soret parameter in the porous layer, $Sr_m = -0.25, -0.1, 0, 0.25, 0.3$. All the graphs show dual effect. In figures 4.7(a) and 4.7(b), increase in Sr_m increases Ra_{T1}, Ra_{T2} in the range $0 \leq \hat{d} \leq 2.2$ showing stabilizing effect and decreases in the range $2.2 \leq \hat{d} \leq 2.6$ showing destabilizing effect. In figure 4.3(c), i.e., for IPSP, increase in Sr_m, increases CRN, Ra_{T3} in the range $0 \leq \hat{d} \leq 2.3$ showing stabilizing effect and decreases in the range $2.3 \leq \hat{d} \leq 2.6$ showing destabilizing effect. Thus the onset of DD-RB convection can be suppressed or augmented depending on the range of the depth ratio for all the three profiles considered.

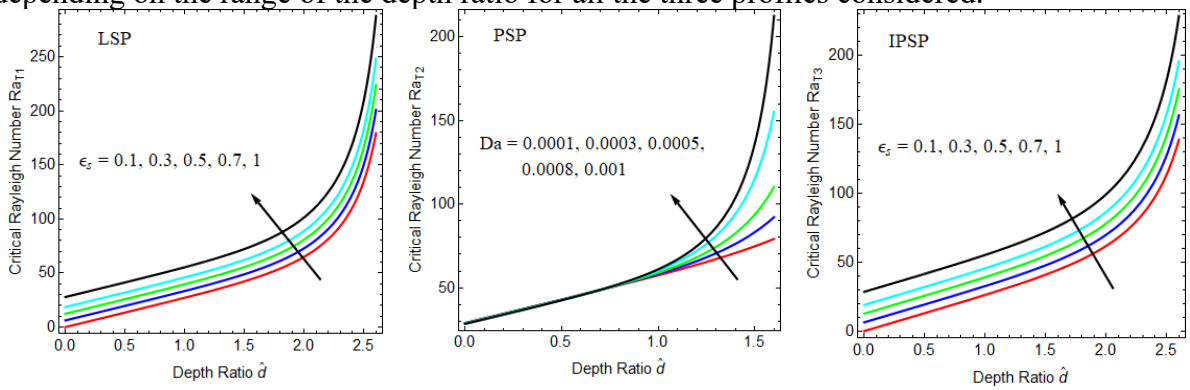

(a)Linear (b)Parabolic (c) Inverted Parabolic

Figure 4.8: Effects of solute diffusivity ratio ϵ_s

Figures 4.8a, 4.8b and 4.8c illustrates the Critical Rayleigh numbers (CRNs) Ra_{T1}, Ra_{T2} and Ra_{T3} versus depth ratio for Linear, Parabolic and Inverted Parabolic salinity profiles by varying Solute diffusivity ratio, $\epsilon_s = 0.1, 0.3, 0.5, 0.7, 1$. The curves are uniformly spaced for all the three profiles. It is observed that as ϵ_s increases the CRNs Ra_{T1}, Ra_{T2} and Ra_{T3} also increases showing stabilizing effect and hence delaying the onset of DD-RB convection for all three profiles.

Figures 4.9a, 4.9b and 4.9c illustrates the Critical Rayleigh numbers (CRNs) Ra_{T1}, Ra_{T2} and Ra_{T3} versus depth ratio for Linear, Parabolic and Inverted Parabolic salinity profiles by varying thermal diffusivity ratio, $\epsilon_T = 0.35, 0.5, 0.6, 0.8, 1$. The curves are uniformly spaced for all the three profiles. It is observed that as ϵ_T increases, the CRNs Ra_{T1}, Ra_{T2} and Ra_{T3}also increases showing stabilizing effect and hence delaying the onset of DD-RB convection for Linear, Parabolic and Inverted Parabolic salinity profiles.

 https://doi.org/10.5281/zenodo.15486315

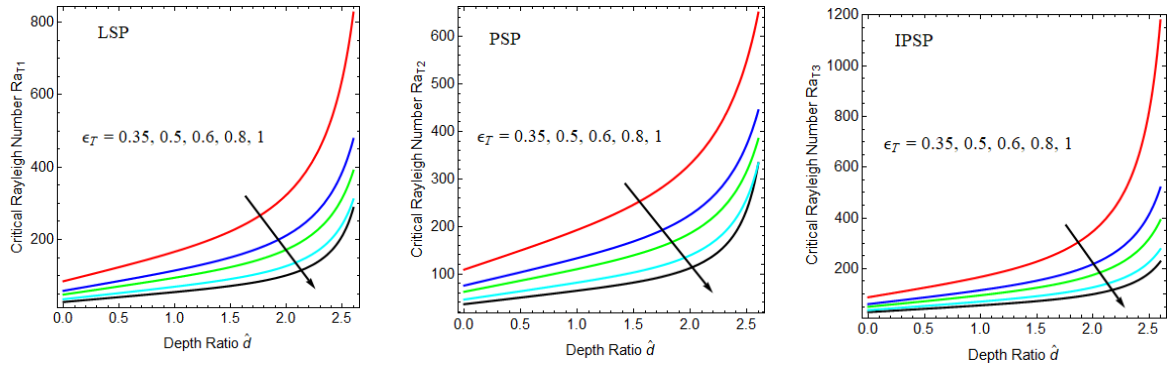

(a)Linear (b)Parabolic (c) Inverted Parabolic

Figure 4.9: Effects of thermal diffusivity ratio ϵ_T

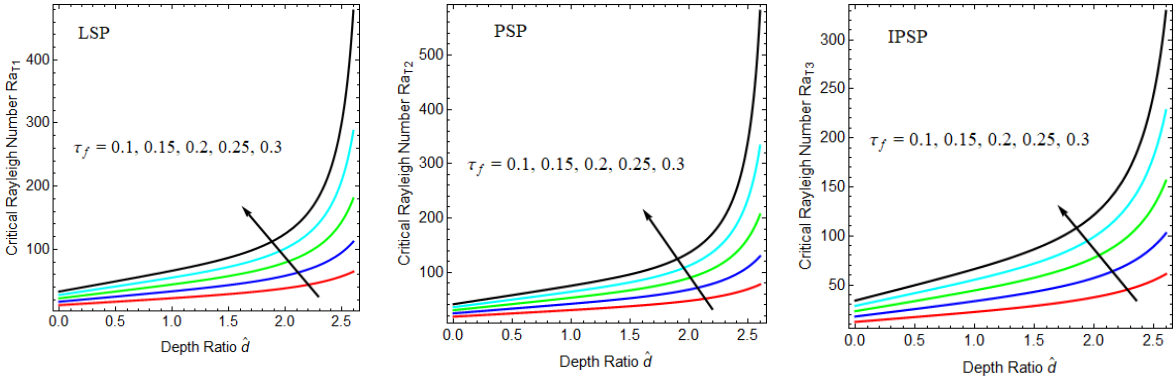

(a)Linear (b)Parabolic (c) Inverted Parabolic

Figure 4.10: Effects of solute to thermal diffusivity ratio in fluid layer τ_f

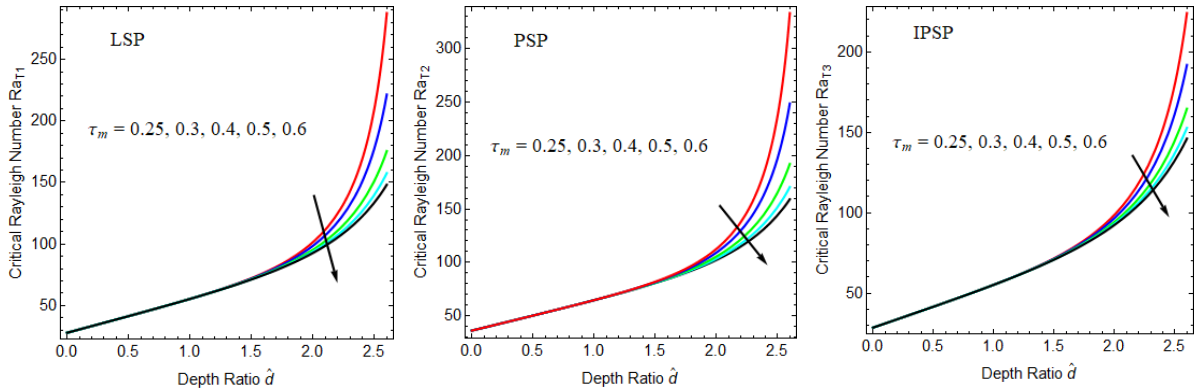

(a)Linear (b)Parabolic (c) Inverted Parabolic

Figure 4.11: Effects of solute to thermal diffusivity ratio in porous layer τ_m

Figures 4.10a, 4.10b and 4.10c illustrates the Critical Rayleigh numbers(CRNs) Ra_{T1}, Ra_{T2} and Ra_{T3} versus depth ratio for Linear, Parabolic and Inverted Parabolic salinity profiles by varying solute to thermal diffusivity ratio in fluid layer, $\tau_f = 0.1, 0.15, 0.2, 0.25, 0.3$. It is observed that as τf increases the CRNs Ra_{T1}, Ra_{T2} and Ra_{T3} also increases showing stabilizing effect and hence delaying the onset of DD-RB convection for Linear, Parabolic and Inverted Parabolic salinity profiles. Also, the curves are diverging for larger values of depth ratio indicating that this parameter is significant in PLDC system.

https://doi.org/10.5281/zenodo.15486315

Figures 4.11a, 4.11b and 4.11c illustrates the Critical Rayleigh numbers (CRNs) Ra_{T1}, Ra_{T2} and Ra_{T3} versus depth ratio for Linear, Parabolic and Inverted Parabolic salinity profiles by varying solute to thermal diffusivity ratio in porous layer, $\tau_m = 0.25, 0.35, 0.4, 0.5, 0.6$. It is observed that as τ_m increases the CRNs Ra_{T1}, Ra_{T2} and Ra_{T3} decreases showing destabilizing effect and hence the onset of DD-RB convection is quickened for LSP, PSP and IPSP. Also, the curves are diverging for larger values of depth ratio indicating that this parameter is significant in PLDC system.

4.1 Conclusion

1. The parabolic salinity profile is the most stable one and inverted parabolic salinity profile is the most unstable salinity profile.
2. The parameters $Da, R_I^*, R_{Im}^*, \tau_f$ and τ_m are crucial in porous dominant composite system.
3. The parameters Da, R_{Im}^*, Ra_S, ϵ_s and τ_f stabilize the composite system.
4. The Soret parameter in the fluid layer Sr_f stabilizes the system for Linear and Parabolic salinity profiles. For inverted parabolic salinity profile, the onset of DDRB convection can be delayed or hastened depending on the range of the depth ratio.
5. The Soret parameter in the porous layer Sr_m is also depth ratio sensitive. That is, depending on the range of the depth ratio, the onset of convection can be suppressed or augmented.
6. The strength of heat source (sink) in the fluid layer represented by modified internal Rayleigh number R_I^* shows stabilizing effect of the composite system for Linear salinity profile, destabilizing effect for Inverted Parabolic salinity profile and dual effect for parabolic salinity profile.
7. By choosing appropriate salinity profile and the range of the depth ratio, the onset of double diffusive Rayleigh-Benard convection can be delayed or hastened.

References

[1] Bhadauria, B. S. (2012). Double-diffusive convection in a saturated anisotropic porous layer with internal heat source. Transport in porous media, 92, 299-320.
[2] Bourich, M., Mamou, M., Hasnaoui, M., & Amahmid, A. (2004). On Stability Analysis of Soret Convection Within a Horizontal Porous Layer: Stability analysis using Galerkin and finite element methods. In Emerging Technologies and Techniques in Porous Media (pp. 221-234). Springer Netherlands.
[3] Capone, F., Gentile, M., Hill, A.A. (2011). Double-diffusive penetrative convection simulated via internal heating in an anisotropic porous layer with throughflow. Int. J. Heat Mass Transf. 54, 1622‑1626.
[4] Chamkha, A. J. (2002). Double-diffusive convection in a porous enclosure with cooperating temperature and concentration gradients and heat generation or absorption effects. Numerical Heat Transfer: Part A: Applications, 41(1), 65-87.
[5] Chen, F. (1992). Salt-finger instability in an anisotropic and inhomogeneous porous substrate underlying a fluid layer. Journal of applied physics, 71(10), 5222-5236.
[6] Chen, F., & Chen, C. F. (1988). Onset of finger convection in a horizontal porous layer underlying a fluid layer. 110(2): 403-409.
[7] Chen, C. F., & Su, T. F. (1992). Effect of surface tension on the onset of convection in a double-diffusive layer. Physics of Fluids A: Fluid Dynamics, 4(11), 2360-2367.
[8] Gobin, D., Goyeau, B., & Songbe, J. P. (1998). Double diffusive natural convection in a composite fluid-porous layer. 120, 234-242.
[9] Charrier-Mojtabi, M. C., Elhajjar, B., & Mojtabi, A. (2007). Analytical and numerical stability analysis of Soret-driven convection in a horizontal porous layer. Physics of Fluids, 19(12). Gangadharaiah, Y. H.

 https://doi.org/10.5281/zenodo.15486315

(2021). Double diffusive surface driven convection in a fluid-porous system. International Journal of Thermofluid Science and Technology, 8, 080301.

[10] Hill, A. A. (2005). Double‐diffusive convection in a porous medium with a concentration based internal heat source. Proceedings of the Royal Society A: Mathematical, Physical and Engineering Sciences, 461(2054), 561-574.

[11] Hirata, S. C., Goyeau, B., & Gobin, D. (2009). Stability of thermosolutal natural convection in superposed fluid and porous layers. Transport in porous media, 78, 525-536.

[12] Haajizadeh, M., Ozguc, A.F., Tien, C.L. (1984): Natural convection in a vertical porous enclosure with internal heat generation. Int. J. Heat Mass Transf. 27, 1893‐1902.

[13] Hardin, G. R., Sani, R. L., Henry, D., & Roux, B. (1990). Buoyancy-driven instability in a vertical cylinder: Binary fluids with Soret effect. Part I: General theory and stationary stability results. International journal for numerical methods in fluids, 10(1), 79-117.

[14] Hardin, G. R., & Sani, R. L. (1993). Buoyancy-driven instability in a vertical cylinder: Binary fluids with Soret effect. Part II: Weakly non-linear solutions. International journal for numerical methods in fluids, 17(9), 755-786.

[15] Jena, S. K., Mahapatra, S. K., & Sarkar, A. (2013). Thermosolutal convection in a fluid-porous composite medium. Heat Transfer—Asian Research, 42(4), 281-299.

[16] Joo, S.W. (1995). Marangoni instabilities in liquid mixtures with Soret effects. Journal of Fluid Mechanics, 293, 127-145.

[17] Joshi, M.V., Gaitonde, U.N., Mitra, S.K. (2006): Analytical study of natural convection in a cavity with volumetric heat generation. ASME J. Heat Transf. 128, 176‐182.

[18] Kim, J., Yong Tae Kang, Chang Kyun Choi.(2007). Soret and Dufour effects on convective instabilities in binary nanofluids for absorption application. International Journal of Refrigeration, Volume 30(2), 323-328.

[19] Malashetty, M. S., & Gaikwad, S. N. (2002). Effect of cross diffusion on double diffusive convection in the presence of horizontal gradients. International journal of engineering science, 40(7), 773-787.

[20] Magyari, E., Pop, I., Postelnicu, A. (2007): Effect of the source term on steady free convection boundary layer flows over a vertical plate in a porous medium, Part I. Transp. Porous Media 67, 49‐67.

[21] Magyari, E., Pop, I., Postelnicu, A. (2007): Effect of the source term on steady free convection boundary layer flows over a vertical plate in a porous medium, Part II. Transp. Porous Media 67, 189‐201.

[22] Manjunatha, N., Sumithra, R., & Vanishree, R. K. (2021). Darcy-Benard double diffusive Marangoni convection in a composite layer system with constant heat source along with non uniform temperature gradients. Malaysian journal of fundamental and applied sciences, 17(1), 7-15.

[23] Mharzi, M., Daguenet, M., & Daoudi, S. (2000). Thermosolutal natural convection in a vertically layered fluid-porous medium heated from the side. Energy conversion and management, 41(10), 1065-1090.

[24] Parthiban, C., Palil, P.R. (1997): Thermal instability in an anisotropic porous medium with internal heat source and inclined temperature gradient. Int. Commun. Heat Mass Transf. 24(7), 1049‐1058.

[25] Parvathy, C.P., Patil, P.R. (1988). Thermohaline instability with thermal diffusion and horizontal gradients. Applied Scientific Research 45, 163‐178.

[26] Schechter, R. S., Prigogine, I., & Hamm, J. R. (1972). Thermal diffusion and convective stability. The Physics of Fluids, 15(3), 379-386.

[27] Singh, A. K., Paul, T., & Thorpe, G. R. (1999). Natural convection due to heat and mass transfer in a composite system. Heat and mass transfer, 35(1), 39-48.

[28] Sumithra, R., Komala, B., & Manjunatha, N. (2020). Darcy-Benard double diffusive Marangoni convection with Soret effect in a composite layer system. Malaya Journal of Matematik, 8(04), 1473-1479.

[29] Sumithra, R., Komala, B., & Manjunatha, N. (2022). The onset of Darcy‐Brinkman‐Rayleigh‐Benard convection in a composite system with thermal diffusion. Heat Transfer, 51(1), 604-620.

[30] Sumithra, R., Archana, M. A., & Acharya, D. R. (2022). Two Component Benard-Marangoni Convection in a Composite System Subjected to Variable Heat Source. Journal of Mines, Metals and Fuels, 70(7A), 53‐63.

[31] Takashima, M. (1976). The Soret Effect on the Thermal Instability of a Two-Component Fluid Layer. Journal of the Physical Society of Japan, 41(4), 1394-1401.

[32] Teamah, M. A. (2008). Numerical simulation of double diffusive natural convection in rectangular enclosure in the presences of magnetic field and heat source. International Journal of Thermal Sciences, 47(3), 237-248.

[33] Rao, Y.F.,Wang, B.X. (1991): Natural convection in vertical porous enclosures with internal heat generation. Int. J. Heat Mass Transf. 34, 247‐252.

[34] Zhao, P., & Chen, C. F. (2001). Stability analysis of double-diffusive convection in superposed fluid and porous layers using a one-equation model. International journal of heat and mass transfer, 44(24), 4625-4633.

 https://doi.org/10.5281/zenodo.15486315